An alternating polymer with fluorinated quinoxaline and 2,7-carbazole segments for photovoltaic devices†

Bo Qu,*[ad] Haimei Wu,[b] Baofeng Zhao,[b] Hongli Liu,[b] Chao Gao,*[b] Xin Qi,[a] Yifan Zhao,[a] Liyang Xuan[a] and Wei Wei[c]

A novel alternating polymer, poly{[*N*-9′-heptadecyl-2,7-carbazole]-*alt*-5,5-[5′,8′-di-2-thienyl-(6′-fluoro-2′,3′-bis-(3″-octyloxyphenyl)-quinoxaline)]} (**PCzFTQx**), based on mono-fluorinated quinoxaline derivative and 2,7-carbazole was synthesized and applied as electron donor material in polymer solar cells. Compared to the corresponding counterpart polymer without fluorine substituent (**PCzTQx**), **PCzFTQx** possesses similar absorption properties and optical bandgap (∼2.0 eV). However, the highest occupied molecular orbital (HOMO) energy level of **PCzFTQx** was lowered to −5.31 eV, about 0.09 eV deeper than that of **PCzTQx**. Benefit from the low-lying HOMO energy level caused by the strong electron deficient fluorine atom on the quinoxaline unit, the optimized photovoltaic device based on **PCzFTQx** and phenyl-C₇₁-butyric acid methyl ester (PC₇₁BM) exhibited an enhanced power conversion efficiency (PCE) of 5.19% with corresponding high open-circuit voltage (V_{oc}) of 0.94 V, relatively to those of 4.72% and 0.82 V for **PCzTQx**-based device. The experimental data indicated that fluorinated quinoxaline based polymer **PCzFTQx** should be a promising donor for polymer solar cells.

1. Introduction

Currently, polymer solar cells (PSCs) with bulk-heterojunction (BHJ) composite layers have attracted broad attention due to their potential applications for large area, low cost, and flexible renewable power sources.[1–4] Although the power conversion efficiency (PCE) of PSCs was already promoted to ∼10%,[5–8] compared with silicon solar cells or other thin-film counterparts, high PCE for PSCs was pursued for its commercialization.[9–11] One key factor to obtain desired photovoltaic properties of PSCs is the development of promising donor conjugated polymers with a broad absorption range and a low-lying highest occupied molecular orbital (HOMO). Furthermore, an interpenetrating network with nano-scale phase separation and a large interfacial area in the donor/acceptor composite layer are also important factors to realize high efficiency of PSCs.[12,13] In order to improve open-circuit voltage (V_{oc}) and PCE of PSCs,

an effective approach is to introduce a strong electron withdrawing group into donor polymer structure and accordingly achieved deep HOMO energy levels.[14,15] For example, ketone, sulfonyl and fluorine atoms, with the characteristics of high electron affinity and none deleterious steric effect, were introduced into conjugated polymers and photovoltaic performance of the solar cells had been optimized.[2,16–20] Moreover, the HOMO and lowest unoccupied molecular orbital (LUMO) energy levels could be lowered by incorporating fluorine atom into copolymers and high V_{oc} of PSCs could be obtained.[21,22]

Quinoxaline is a common-used electron-withdrawing moiety and the HOMO and band gaps of the quinoxaline-based alternating polymers could be effectively modulated due to the tunable structure of quinoxaline unit.[23–25] Therefore, fluorinated quinoxaline-based alternating polymers showed low-lying HOMO and improved photovoltaic performance.[26–31] Herein, a new alternating polymer poly{[*N*-9′-heptadecyl-2,7-carbazole]-*alt*-5,5-[5′,8′-di-2-thienyl-(6′-fluoro-2′,3′-bis-(3″-octyloxyphenyl)-quinoxaline)]} (**PCzFTQx**) based on mono-fluorinated quinoxaline and 2,7-carbazole derivative was synthesized. Benefit from its lowered HOMO energy level (−5.31 eV), about 0.09 eV deeper than that of the non-fluorinated counterpart[32] (named as **PCzTQx** in this work), a remarkable V_{oc} (0.94 V) and PCE (5.19%) were obtained for **PCzFTQx** : phenyl-C₇₁-butyric acid methyl ester (PC₇₁BM)-based PSCs, which were 10% and 12% larger than those of the analogue **PCzTQx**-based devices under the same condition. The experimental data implied that **PCzFTQx** would be a promising donor copolymer for PSCs in future.

[a]*State Key Laboratory for Artificial Microstructures and Mesoscopic Physics, Department of Physics, Peking University, Beijing, 100871, People's Republic of China. E-mail: bqu@pku.edu.cn; Tel: +86-10-62766902*

[b]*Xi'an Modern Chemistry Research Institute, Xi'an, Shaanxi, 710065, People's Republic of China. E-mail: chaogao74@gmail.com*

[c]*Institute of Advanced Materials, Nanjing University of Posts and Telecommunications, Nanjing, 210003, People's Republic of China*

[d]*New Display Device and System Integration Collaborative Innovation Center of the West Coast of the Taiwan Strait, Fuzhou, 350002, People's Republic of China*

† Electronic supplementary information (ESI) available. See DOI: 10.1039/c6ra28128a

2. Experimental

2.1 Materials and characterization

All chemicals and solvents were purchased from Aldrich or Alfa & Aesar. Tetrahydrofuran (THF) is dried over Na/benzophenone ketyl and freshly distilled prior to use. 5,8-Bis((5-bromothiophen-2-yl)-2,3-bis(3-octyloxy)phenyl)quinoxaline (M1) and 5,8-bis((5-bromothiophen-2-yl)-6-fluoro-2,3-bis(3-octyloxy)phenyl)quinoxaline (M2) that followed our previous work[27] were prepared. 2,7-Bis(4',4',5',5'-tetramethyl-1',3',2'-dioxaborolan-2'-yl)-N-9''-heptadecanylcarbazole (M3)[33] were synthesized according to the reported literatures. The synthetic routes of monomers and copolymers are given in Scheme 1.

2.2 Synthesis of PCzFTQx and PCzTQx

In a 50 mL dry flask, monomer M1 (175.7 mg, 0.2 mmol) or M2 (172.2 mg, 0.2 mmol) and 2,7-bis(4',4',5',5'-tetramethyl-1',3',2'-dioxaborolan-2'-yl)-N-9''-heptadecanyl-carbazole M3 (131.5 mg, 0.2 mmol) were dissolved in a mixture of 20% aqueous tetraethylammonium hydroxide (1.5 mL) and degassed toluene (10 mL). The mixture was flushed with nitrogen for 30 min. Tris-(dibenzylideneacetone)dipalladium(0) (Pd$_2$(dba)$_3$) (3.7 mg) and tri(o-tolyl)phosphine (P(o-Tol)$_3$) 6.5 mg were added, flushed with nitrogen again. Then the mixture was vigorously stirred at 100 °C for 48 h under a nitrogen atmosphere. The polymer was end-capped by adding phenyl boronic acid (2.4 mg) and bromobenzene (2.2 μL) at the end of polymerization. After cooling to room temperature, the solution was poured into methanol. The obtained polymer was then subjected to Soxhlet-extracted with methanol, hexane and chloroform successively. The chloroform solution was concentrated to a small volume, and precipitated by pouring this solution into methanol. Finally, the polymer was collected by filtration, dried under vacuum at 50 °C overnight.

For PCzTQx. (148 mg, yield 67.1%). ^{1}H NMR (CDCl$_3$, 500 MHz) δ (ppm): 8.22 (br, 2H), 7.98 (br, 2H), 7.71 (br, 6H), 7.48 (br, 4H), 7.36 (br, 4H), 7.01 (d, 2H, J = 10 Hz), 3.95–3.86 (br, 5H). Gel permeation chromatography (GPC, as shown in Fig. S1 in the ESI†) (tetrahydrofuran, polystyrene standard): M_n = 9.93 kDa, M_w = 17.89 kDa, PDI = 1.80. Anal. calcd for (C$_{73}$H$_{89}$N$_3$O$_2$S$_2$)$_n$ (%): C 79.37, H 8.12, N 3.80. Found (%): C 77.77, H 7.86, N 3.77.

For PCzFTQx. (155 mg, 69.2% yield). ^{1}H NMR (CDCl$_3$, 500 MHz) δ (ppm): 8.22 (br, 1H), 7.96 (br, 2H), 7.72 (br, 6H), 7.48 (br, 4H), 7.36 (br, 4H), 7.00 (d, 2H, J = 8 Hz), 3.95–3.86 (br, 5H). GPC (tetrahydrofuran, polystyrene standard): M_n = 54.37 kDa, M_w = 127.79 kDa, PDI = 2.35. Anal. calcd for (C$_{73}$H$_{88}$N$_3$O$_2$FS$_2$)$_n$ (%): C 78.10, H 7.90, N 3.74. Found (%): C 77.99, H 7.80, N 3.53.

2.3 Characterization

All the compounds were characterized by nuclear magnetic resonance spectra (NMR) recorded (Bruker AV 500 spectrometer) in chloroform-d (CDCl$_3$) at room temperature using tetramethylsilane (TMS) as an internal reference. The chemical shifts were accounted in ppm related to the singlet of CDCl$_3$ at 7.26 ppm for ^{1}H NMR. Molecular weights and distributions of the copolymers were estimated by gel permeation chromatography (GPC) method, tetrahydrofuran (THF) as eluent and polystyrene as standard. The absorption spectra and thermogravimetric analysis (TGA, as shown in Fig. S2 in the ESI†) were measured with a Unico UV-2102 scanning spectrophotometer and a Universal V2.6D TA instrument, respectively. The electrochemical cyclic voltammetry (CV) was determined by a CHI 660D Electrochemical Workstation with glassy carbon, Pt wire, and Ag/Ag$^+$ electrodes as the working electrode, counter electrode, and reference electrode respectively in a 0.1 mol L^{-1} tetrabutylammonium hexafluorophosphate (Bu$_4$NPF$_6$) acetonitrile solution. Polymers in chloroform solution (analytical reagent, 2 mg mL^{-1}) were drop casted onto working electrode and dried in air at room temperature. Atomic force microscopy (AFM) measurement of the surface morphology of samples was conducted in air under ambient condition using the PicoPlus microscope (Agilent).

2.4 PSCs fabrication and characterization

PSCs with the configuration of ITO/PEDOT : PSS/ PCzFTQx : PC$_{71}$BM/poly[(9,9-bis(3'-(N,N-dimethylamino)propyl)-2,7-fluorene)-alt-2,7-(9,9-dioctylfluorene)] (PFN)/Al were fabricated and characterized in this work. With varying the weight ratio of PCzFTQx : PC$_{71}$BM from 1 : 1 to 1 : 4, the photovoltaic properties of PSCs were systematically investigated. For comparison, the control device based on PCzTQx : PC$_{71}$BM (1 : 3) (the optimal specimen in the previous literature[32]) was also prepared with the same configuration and experimental condition in this work.

ITO-coated glass with sheet resistance of ~15 Ω per square (Ω □$^{-1}$) was used as the anode. The ITO glass was ultrasonically cleaned with detergent, distilled water, acetone, isopropyl alcohol, and then treated with ultraviolet-ozone (Ming Heng, PDC-MG) for 20 min. Then a 40 nm thick PEDOT : PSS (Clevios P VP AI 4083, H. C. Starck Inc.) layer was spin-coated from an aqueous solution onto ITO substrates, followed by being annealed at 120 °C for 30 min on a hotplate in air. The substrates were transferred into a nitrogen-filled glove box. Then the photoactive layers were prepared by spin-coating
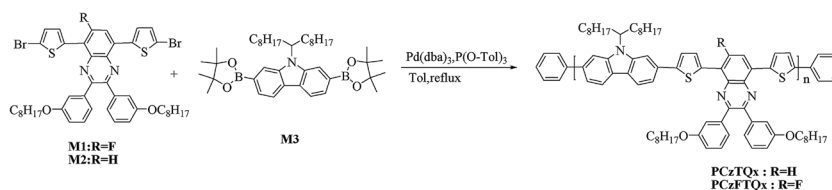
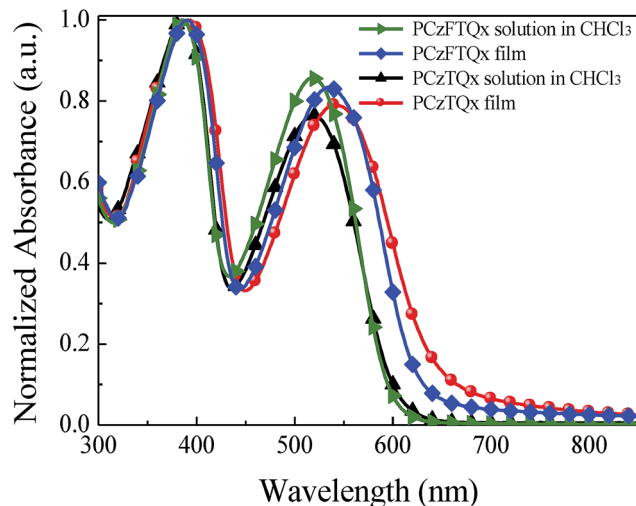Scheme 1 Synthetic route of PCzFTQx and PCzTQx.
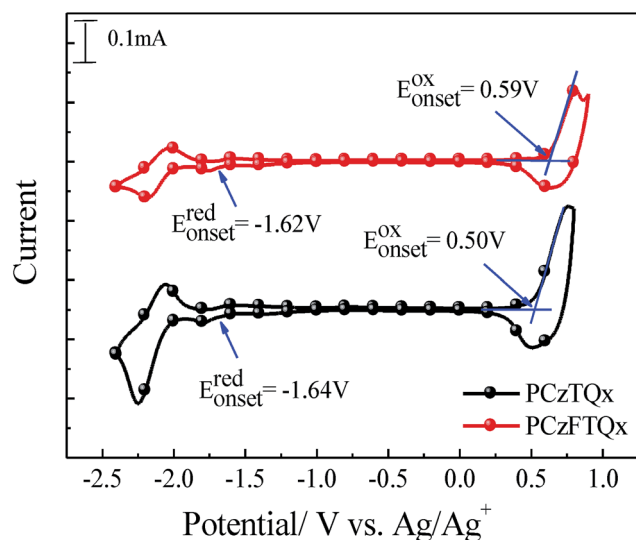
Fig. 1 Absorption spectra of **PCzFTQx** and **PCzTQx**.

Fig. 2 Cyclic voltammogram of **PCzFTQx** and **PCzTQx** films on glassy carbon electrode (0.1 mol L^{-1} Bu$_4$NPF$_6$, acetonitrile solution with a scan rate of 100 mV s^{-1}).

(1000 rpm, 30 s) a blend solution of the polymer and PC$_{71}$BM in *ortho*-dichlorobenzene (*o*DCB) on the top of ITO/PEDOT : PSS substrates. The thickness of the photoactive layers was controlled in the range of 80–100 nm. A 5 nm PFN layer was then spin-coated from methanol solution in the presence of a trace amount of acetic acid onto the active layer. The thin PFN layer was employed as the cathode interlayer since it could improve the electron extraction.[6] Finally, the substrates were
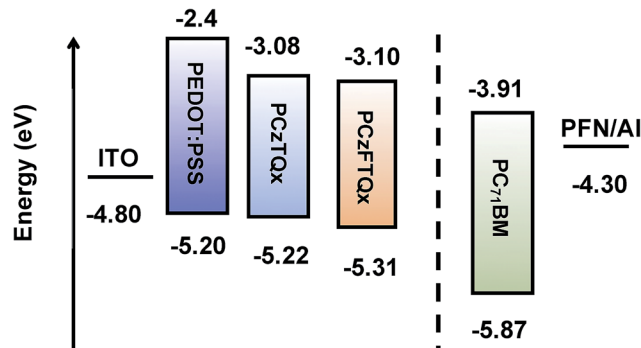

Fig. 3 Schematic illustration of relative positions of HOMO/LUMO energy levels of the materials in the PSCs.

transferred into a vacuum chamber and Al cathodes (~120 nm) were thermally deposited onto the substrates. The effective area of PSCs was ~0.16 cm^2 controlled by the shadow mask. The photovoltaic properties of PSCs were recorded by *J–V* measurement (using a Keithley 2400 source meter) under 1 sun, AM 1.5G spectrum from a solar simulator (Newport model 94021A, 100 mW cm^{-2}). A monocrystal silicon cell (VLSI Standards Inc.) calibrated by the National Renewable Energy Laboratory (NREL) is used as a reference. The incident photo to current conversion efficiency spectra were measured by using a Hypermonolight System (QTEST 1000 AD, Crowntech Inc.).

3. Results and discussion

3.1 Thermal properties

As shown in the TGA curves of the polymers (Fig. S2 in the ESI†), the thermal decomposition temperature (5% weight loss) of **PCzFTQx** was about 403 °C, slightly lower than that of **PCzTQx** (405 °C), indicating its good thermal stability for photovoltaic applications.

3.2 Absorption properties

The normalized UV-vis absorption spectra of **PCzFTQx** and **PCzTQx** in chloroform (CHCl$_3$) solution and film states were exhibited in Fig. 1. The absorption peaks of **PCzFTQx** and **PCzTQx** in CHCl$_3$ solution were almost identical. The peaks located at 386 nm and 517 nm, which were attributed to the absorption of carbazole segment and intramolecular charge transfer, respectively.[32] As to the film state, the absorption peaks of **PCzFTQx** and **PCzTQx** in the long wavelength region were red shifted to 536 nm and 542 nm, respectively. The weak bathochromic shift effect of the polymers from solution state to film state implied that the aggregation and chain–chain stacking of **PCzFTQx** and **PCzTQx** were relatively limited. The optical band gap (E_g^{opt}) of the polymers

Table 1 Electrochemical potentials and energy levels of **PCzFTQx** and **PCzTQx**

Polymers	E_{onset}^{ox} (V)	E_{onset}^{red} (V)	E_{HOMO} (eV)	E_{LUMO} (eV)	E_g^{ec} (eV)	E_g^{opt} (eV)
PCzFTQx	0.59	−1.62	−5.31	−3.10	2.21	2.04
PCzTQx	0.50	−1.64	−5.22	−3.08	2.14	1.98

was calculated to be 2.04 eV for **PCzFTQx** and 1.98 eV for **PCzTQx** from the absorption onset of the films.

3.3 Electrochemical properties

In order to study the electrochemical properties of the polymers, cyclic voltammetry (CV) was carried out using an electrochemical workstation. CV curves of **PCzFTQx** and **PCzTQx** films were measured as shown in Fig. 2. The level of ferrocene/ferrocenium (Fc/Fc$^+$) was −4.72 eV below the vacuum level.[29] The former potential of Fc/Fc$^+$ was ∼0.08 eV against Ag/Ag$^+$. The onset oxidation and reduction potential of **PCzFTQx** film located at 0.59 V and −1.62 V, respectively. Therefore, the

PCzTQx ; **PCzFTQx**

LUMO+1=-2.13 eV LUMO+1= -2.19 eV

LUMO= -2.23 eV LUMO= -2.26 eV

HOMO=-4.59 eV HOMO=-4.64 eV
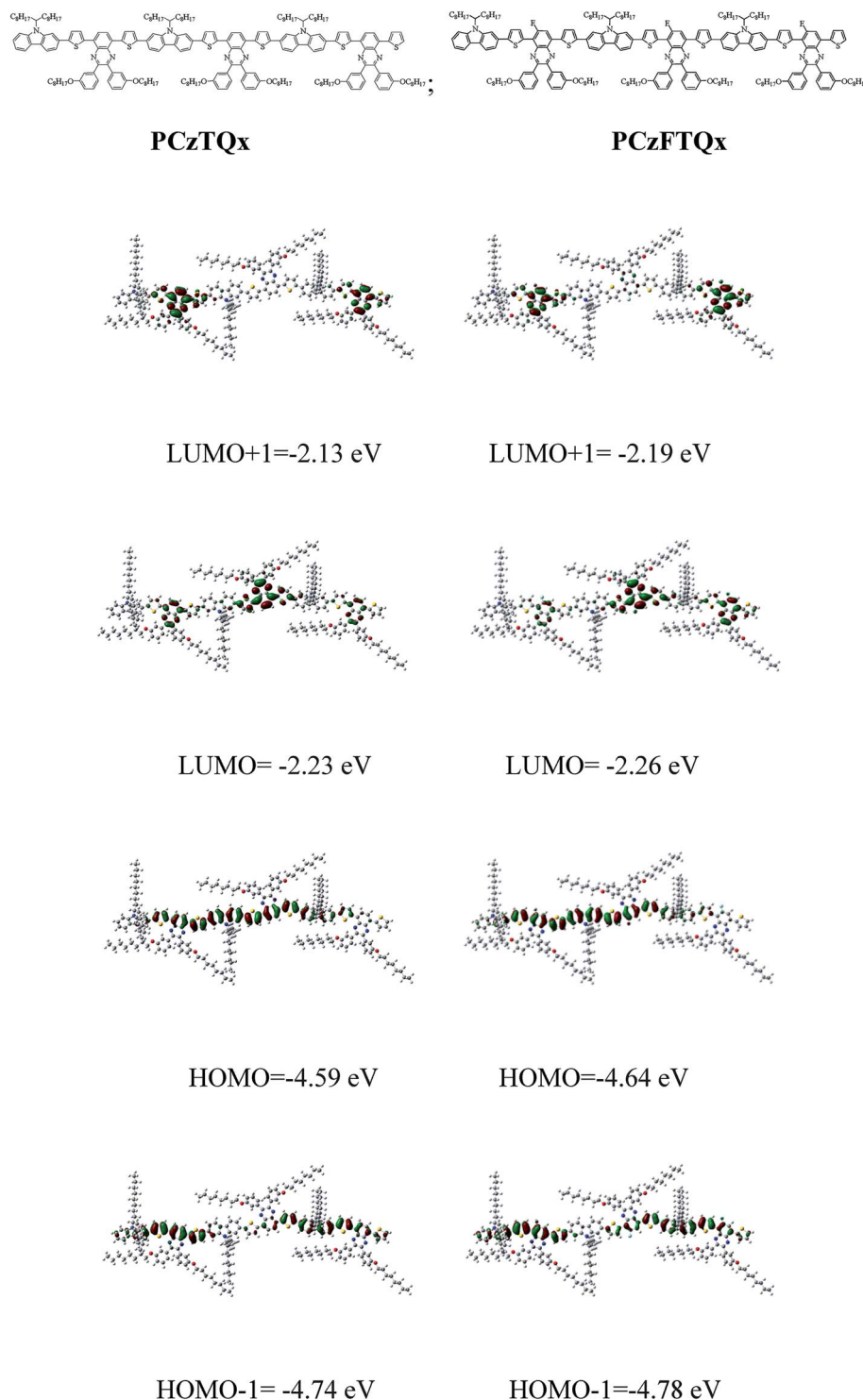
HOMO-1= -4.74 eV HOMO-1=-4.78 eV

Fig. 4 Molecular structures and electron density of LUMO+1, LUMO, HOMO and HOMO−1 for **PCzTQx** and **PCzFTQx** computed at the B3LYP/6-31G* level.

HOMO and LUMO of **PCzFTQx** were evaluated to be −5.31 eV and −3.10 eV, respectively. The electrochemical energy band gap (E_g^{ec}) of **PCzFTQx** film was calculated to be 2.21 eV. Although E_g^{ec} value was a little bit larger than E_g^{opt} (2.04 eV) estimated from the UV-vis spectra, it was still in the range of error (0.1–0.5 eV). As to **PCzTQx** film, the HOMO and LUMO were measured to be −5.22 eV and −3.08 eV, respectively. The E_g^{ec} and E_g^{opt} of **PCzTQx** were 2.14 eV and 1.98 eV, slightly smaller than those of **PCzFTQx**. The energy level data were summarized in Table 1 and the schematic illustration of energy levels of **PCzFTQx**, **PCzTQx**, $PC_{71}BM$[34] and PEDOT : PSS[35] was depicted in Fig. 3. The HOMO of **PCzFTQx** was ∼0.09 eV deeper than that of **PCzTQx**, which was ascribed to the introduction of fluorine atom onto the quinoxaline segment in **PCzFTQx**.[27,29] Therefore, the gap between the HOMO level of **PCzFTQx** and LUMO level of $PC_{71}BM$ was as large as 1.40 eV, which facilitated high V_{oc} of photovoltaic devices. Moreover, the LUMO level of **PCzFTQx** was ∼0.81 eV higher than that of $PC_{71}BM$, then electrons could transfer automatically at the donor/acceptor interface.

3.4 Theoretical calculations

Quantum chemistry calculation by the DFT (B3LYP/6-31G* level) method was employed to demonstrate the electronic structures of the **PCzTQx** and **PCzFTQx**. Three repeat units were chosen as the model compounds for the simulations of **PCzTQx** and **PCzFTQx**, and the actual long alkyl groups were kept without simplification. As shown in Fig. 4, the electron density in HOMO orbitals distributed along the whole backbone despite somewhat more intensely at carbazole conjugated units and less at quinoxaline units. However, the electron density in LUMO orbitals mainly localized at the quinoxaline units. The HOMO−1 electron density distributed more intensely in π-bridge thiophene and carbazole conjugated units, while the LUMO+1 electron density distributed more intensely at the quinoxaline units. The electron density distribution of the different orbitals implied that the internal charge transfers were possible in the conjugated systems. It should be noted that the F atom that incorporated onto the quinoxaline unit showed significant effect on the HOMO and LUMO energy levels of **PCzFTQx** (−4.64 eV/−2.26 eV). The additional F atoms depressed both HOMO and LUMO energy levels, which agreed well with the trend of electrochemical results.

3.5 Photovoltaic properties

In order to study the photovoltaic properties of **PCzFTQx**, PSCs with the conventional structure of ITO/PEDOT : PSS/**PCzFTQx** : $PC_{71}BM$/PFN/Al were fabricated. **PCzFTQx** was used as the electron donor and $PC_{71}BM$ as the electron acceptor. Chlorobenzene was used as the solvent to prepare the **PCzFTQx** : $PC_{71}BM$ blend films. The weight ratio of **PCzFTQx** : $PC_{71}BM$ was changed from 1 : 1 to 1 : 4 and J–V curves of PSCs were modulated accordingly as shown in Fig. 5. When the weight ratio of **PCzFTQx** : $PC_{71}BM$ reached 1 : 3, the PSC exhibited a reasonable photovoltaic performance as shown in Table 2 and the V_{oc}, J_{sc}, FF and PCE values were evaluated to be 0.94 V, 9.71 mA cm^{-2}, 0.56 and 5.09%, respectively. As
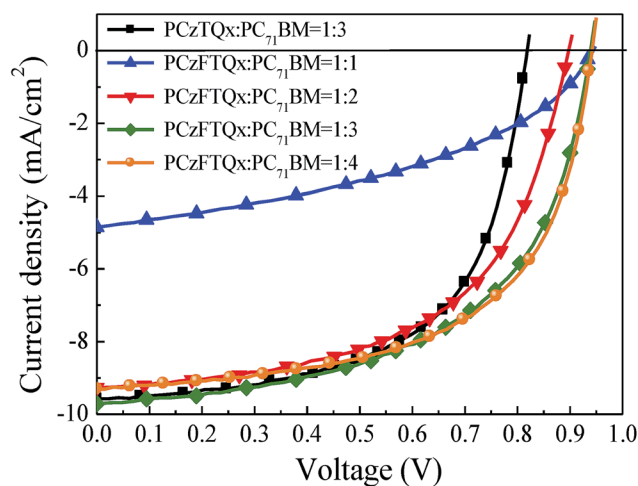

Fig. 5 Current density *vs.* voltage characteristics of PSCs under AM 1.5G irradiation of 100 mW cm^{-2}.

Table 2 Photovoltaic data of the polymer solar cells

PCzFTQx : $PC_{71}BM$[a]	V_{oc} (V)	J_{sc} (mA cm^{-2})	FF	PCE (%)
1 : 1	0.94	4.86	0.42	1.92
1 : 2	0.90	9.27	0.57	4.70
1 : 3	0.94	9.71	0.56	4.09
1 : 4	0.94	9.31	0.59	5.19
PCzTQx : $PC_{71}BM$ (1 : 3)[a]	0.82	9.57	0.60	4.72

[a] The thickness of the active layer was in the range of 80–100 nm.

expected, the PSC based on **PCzFTQx** : $PC_{71}BM$ (1 : 3) has higher V_{oc} and PCE than those of the corresponding **PCzTQx**-based device (blend ratio of 1 : 3),[32] which was ascribed to the introduction of fluorine atom into the polymer and the low-lying HOMO level of **PCzFTQx**. It was worthy to note that the PSC with **PCzFTQx** : $PC_{71}BM$ (1 : 3) as the active layer exhibited the highest J_{sc} of 9.71 mA cm^{-2} in this work, approximately 0.14 mA cm^{-2} higher than that of **PCzTQx** control device. Moreover, when the weight ratio of **PCzFTQx** : $PC_{71}BM$ reached 1 : 4, the highest PCE of 5.19% was achieved, mainly due to the increased FF of 0.59. Therefore, the PCE value was almost unaltered when the ratio of **PCzFTQx** : $PC_{71}BM$ changed from 1 : 3 to 1 : 4.

The external quantum efficiency (EQE) curves were also recorded to characterize the photovoltaic properties of the PSCs as shown in Fig. 6. The EQE curves covered from 350 nm to 650 nm, which matched well with the absorption range of the organic photoactive layers. Compared with any other **PCzFTQx** : $PC_{71}BM$-based devices with different blend ratios, the **PCzFTQx** : $PC_{71}BM$ (1 : 3)-based device exhibited a high EQE value up to 62%, leading to a high short circuit current density of 9.71 mA cm^{-2}.

Atomic force microscopy (AFM) was conducted to evaluate the phase-separated morphologies of the blend films and the topography images (5 μm × 5 μm) of **PCzTQx** : $PC_{71}BM$ (1 : 3) and **PCzFTQx** : $PC_{71}BM$ (1 : 4) corresponding to the best photovoltaic performance were shown in Fig. 7. The
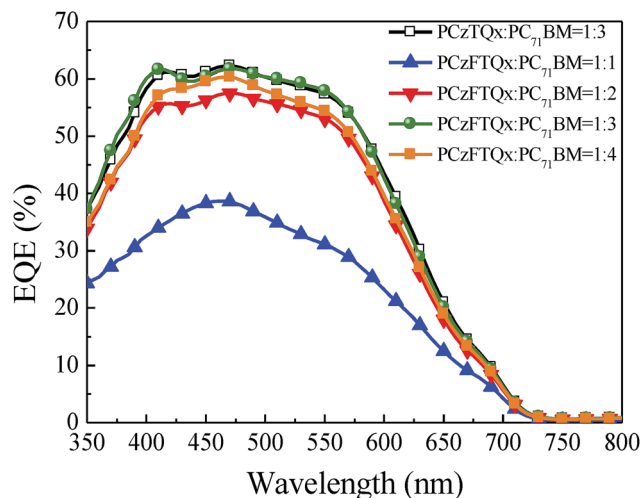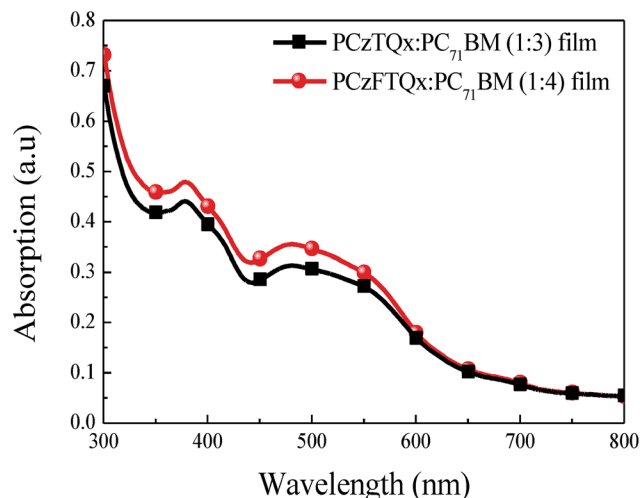
Fig. 6 EQE spectra of the PSCs.

Fig. 8 Absorption spectra of **PCzTQx** : $PC_{71}BM$ (1 : 3) and **PCzFTQx** : $PC_{71}BM$ (1 : 4) films.

interpenetrating feature with bicontinuous network between the polymer and $PC_{71}BM$ was realized for both the two blend films. **PCzTQx** : $PC_{71}BM$ blend film showed a relatively smooth surface with a root-mean-square roughness (RMS) of 2.99 nm and an ideal domain size of 10–20 nm, which were favorable for efficient diffusion of excitons to donor–acceptor interfaces.[36,37] However, for the fluorinated polymer **PCzFTQx**-based blend film, RMS value was enlarged (5.27 nm) with the corresponding domain size of 40–60 nm, which was somewhat larger than the typical exciton diffusion length of *ca.* 10 nm,[13] thus was not desired for efficient exciton dissociation at the D/A interfaces.

To get insight into the charge transporting property of the two polymers, the hole-only devices were fabricated to measure the hole mobility using the space-charge-limited current (SCLC) method. The hole-only devices employed the structure of ITO/ PEDOT : PSS/polymer : $PC_{71}BM$/MoO_3/Al. And the *J–V* characteristics of the hole-only devices were measured and fit the dark current using the SCLC model, which was described by the equation: $J = \frac{9}{8}\varepsilon_0\varepsilon\mu\frac{(V_{app} - V_s - V_{bi})^2}{L^3}$, where *J* was the current density, ε_0 was the permittivity of free space, ε was the relative

permittivity of polymers, μ was the charge carrier mobility, V_{app} was the applied voltage, V_s was the voltage drop from the substrate's series resistance and V_{bi} was the built-in voltage. As illustrated in Fig. S3,† the hole (μ_h) mobilities were calculated through the slope of the $J^{1/2}$–V curves, which were exhibited in Table S1.† Relative to the μ_h value of 3.12×10^{-5} cm^2 V^{-1} s^{-1} for **PCzTQx**, the fluorinated polymer **PCzFTQx** showed slightly high μ_h value of 6.18×10^{-5} cm^2 V^{-1} s^{-1}, which was consistent with the experimental data of the previous literature.[22] And the high μ_h of **PCzFTQx** was beneficial to the photovoltaic performance of the corresponding devices.

The absorption spectra of **PCzTQx** : $PC_{71}BM$ and **PCzFTQx** : $PC_{71}BM$ active layers under the optimal weight ratios were recorded in Fig. 8. It can be seen that in the region from 300 nm to 440 nm, the **PCzFTQx** blend film showed slightly high absorption property, which was mainly resulted from the high ratio of $PC_{71}BM$ in the blend film. In addition, a little stronger absorption for **PCzFTQx** blend film in the range of 440–600 nm might be ascribed to the slightly enhanced absorption behavior of **PCzFTQx** pristine film in this region as
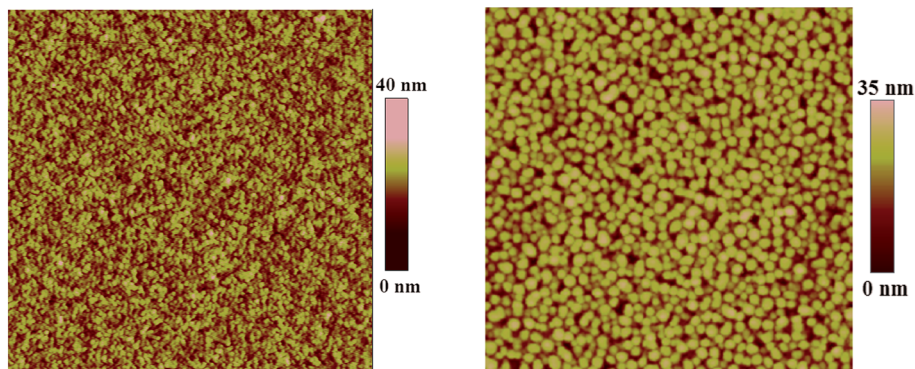

Fig. 7 AFM topography images (5 μm × 5 μm) of ITO/PEDOT : PSS/**PCzTQx** : $PC_{71}BM$ (1 : 3) (left, RMS = 2.99 nm), and ITO/PEDOT : PSS/ **PCzFTQx** : $PC_{71}BM$ (1 : 4) (right, RMS = 5.27 nm).

seen in Fig. 1, which would be benefit to the improvement of photocurrent. As described ahead, the domain size of **PCzFTQx** : PC$_{71}$BM blend film was larger to some extent and not suitable for the efficient exciton dissociation. Then, the J_{sc} of the corresponding **PCzFTQx** : PC$_{71}$BM based device was 9.31 mA cm^{-2}, almost equal to that of **PCzTQx**:PC$_{71}$BM based device. Therefore, if further improvement of morphology can be adopted to obtain ideal domain size and phase separation, enhanced photovoltaic performance may be anticipated for **PCzFTQx** based solar cells.

4.   Conclusions

A novel copolymer **PCzFTQx** with mono-fluorinated quinoxaline derivative and 2,7-carbazole segment was reported and the photovoltaic properties of **PCzFTQx** were investigated in this work. Due to the introduction of fluorine atom in quinoxaline unit, **PCzFTQx** exhibited a lowered HOMO level (-5.31 eV), about 0.09 eV deeper than that of the non-fluorinated counterpart **PCzTQx** (-5.22 eV). High V_{oc} (0.94 V) and PCE (5.19%) were achieved for the optimized **PCzFTQx** : PC$_{71}$BM-based PSCs, which were 12% and 10% larger than those of the non-fluorinated analogue **PCzTQx**-based devices. Therefore, the fluorine atom in **PCzFTQx** was an effective electron-withdrawing unit and the accompanying beneficial modulation of the energy levels for **PCzFTQx** was realized accordingly. Hence, **PCzFTQx** showed remarkable photovoltaic properties and would be a promising donor candidate for PSCs and other optoelectronic devices.

Acknowledgements

Notes and references

1 C. W. Tang, *Appl. Phys. Lett.*, 1986, **48**, 183–185.
2 J. Hou, H. Y. Chen, S. Zhang, R. I. Chen, Y. Yang, Y. Wu and G. Li, *J. Am. Chem. Soc.*, 2009, **131**, 15586.
3 B. Qu, Z. Jiang, Z. Chen, L. Xiao, D. Tian, C. Gao, W. Wei and Q. Gong, *J. Appl. Polym. Sci.*, 2012, **124**, 1186–1192.
4 H. X. Zhou, L. Q. Yang, S. C. Price, K. J. Knight and W. You, *Angew. Chem., Int. Ed.*, 2010, **49**, 7992–7995.
5 Y. H. Liu, J. B. Zhao, Z. K. Li, C. Mu, W. Ma and H. W. Hu, *Nat. Commun.*, 2014, **5**, 5293.
6 Z. C. He, B. Xiao, F. Liu, H. B. Wu, Y. L. Yang, S. Xiao, C. Wang, T. P. Russell and Y. Cao, *Nat. Photonics*, 2015, **9**, 174–179.
7 X. Ouyang, R. Peng, L. Ai, X. Zhang and Z. Ge, *Nat. Photonics*, 2015, **9**, 520–524.
8 L. Nian, W. Zhang, N. Zhu, L. Liu, Z. Xie, H. Wu, F. Wuerthner and Y. Ma, *J. Am. Chem. Soc.*, 2015, **137**, 6995–6998.
9 Y. J. Cheng, S. H. Yang and C. S. Hsu, *Chem. Rev.*, 2009, **109**, 5868–5923.
10 J. W. Chen and Y. Cao, *Acc. Chem. Res.*, 2009, **42**, 1709–1718.
11 G. D. Dennler, M. C. Scharber and C. J. Brabec, *Adv. Mater.*, 2009, **21**, 1323–1338.
12 G. Li, V. Shrotriya, J. S. Huang, Y. Yao, T. Moriarty, K. Emery and Y. Yang, *Nat. Mater.*, 2005, **4**, 864–868.
13 J. Peet, J. Y. Kim, N. E. Coates, W. L. Ma, D. Moses, A. J. Heeger and G. C. Bazan, *Nat. Mater.*, 2007, **6**, 497–500.
14 M. L. Keshtov, S. A. Kuklin, F. C. Chen, A. R. Khokhlov, R. Kurchania and G. D. Sharma, *J. Polym. Sci., Part A: Polym. Chem.*, 2015, **53**, 2390–2398.
15 T. L. Wang, S. C. Huang, C. H. Yang, Y. Y. Chuang and C. H. Chen, *eXPRESS Polym. Lett.*, 2015, **9**, 881–893.
16 Y. Huang, L. Huo, S. Zhang, X. Guo, C. C. Han, Y. Li and J. Hou, *Chem. Commun.*, 2011, **47**, 8904–8906.
17 S. C. Price, A. C. Stuart, L. Q. Yang, H. X. Zhou and W. You, *J. Am. Chem. Soc.*, 2011, **133**, 4625–4631.
18 H. J. Son, B. Carsten, I. H. Jung and L. P. Yu, *Energy Environ. Sci.*, 2012, **5**, 8158–8170.
19 H. Y. Chen, J. H. Hou, S. Q. Zhang, Y. Y. Liang, G. W. Yang, Y. Yang, L. P. Yu, Y. Wu and G. Li, *Nat. Photonics*, 2009, **3**, 649–653.
20 Y. Y. Liang, Z. Xu, J. B. Xia, S. T. Tsai, Y. Wu, G. Li, C. Ray and L. P. Yu, *Adv. Mater.*, 2010, **22**, E135–E138.
21 D. Dang, W. Chen, R. Yang, W. Zhu, W. Mammod and E. Wang, *Chem. Commun.*, 2013, **49**, 9335–9337.
22 H. J. Son, W. Wang, T. Xu, Y. Liang, Y. Wu, G. Li and L. Yu, *J. Am. Chem. Soc.*, 2011, **133**, 1885–1894.
23 E. G. Wang, L. T. Hou, Z. Q. Wang, S. Hellstr, F. L. Zhang, O. Ingan and M. R. Andersson, *Adv. Mater.*, 2010, **22**, 5240–5244.
24 Y. H. Fu, H. Cha, S. Song, G. Y. Lee, C. E. Park and T. Park, *J. Polym. Sci., Part A: Polym. Chem.*, 2013, **51**, 372–382.
25 H. Wu, B. Qu, Z. Cong, H. Liu, D. Tian, B. Gao, Z. An, C. Gao, L. Xiao, Z. Chen, H. Liu, Q. Gong and W. Wei, *React. Funct. Polym.*, 2012, **72**, 897–903.
26 Z. Gao, B. Qu, H. Wu, H. Yang, C. Gao, L. Zhang, L. Xiao, Z. Chen, W. Wei and Q. Gong, *Synth. Met.*, 2013, **172**, 69–75.
27 H. Wu, B. Qu, D. Tian, Z. Cong, B. Gao, J. Liu, Z. An, C. Gao, L. Xiao, Z. Chen, Q. Gong and W. Wei, *React. Funct. Polym.*, 2013, **73**, 1432–1438.
28 Z. Cong, B. Zhao, H. Wu, Z. Guo, W. Wang, G. Luo, J. Xu, Y. Xia, C. Gao and Z. An, *Polymer*, 2015, **67**, 55–62.
29 Y. Lu, Z. Xiao, Y. Yuan, H. Wu, Z. An, Y. Hou, C. Gao and J. Huang, *J. Mater. Chem. C*, 2013, **1**, 630–637.
30 J. Yuan, L. Qiu, Z. Zhang, Y. Li, Y. Chen and Y. Zou, *Nano Energy*, 2016, **30**, 312–320.
31 J. Yuan, L. Qiu, Z. Zhang, Y. Li, Y. He, L. Jiang and Y. Zou, *Chem. Commun.*, 2016, **52**, 6881–6884.
32 E. Wang, L. Hou, Z. Wang, Z. Ma, S. Hellstrom, W. Zhuang, F. Zhang, O. Inganas and M. R. Andersson, *Macromolecules*, 2011, **44**, 2067–2073.
33 Y. Li, J. Ding, M. Day, Y. Tao, J. Lu and M. D'iorio, *Chem. Mater.*, 2004, **16**, 2165–2173.

34 P. Dutta, W. Yang, S. H. Eom and S. H. Lee, *Org. Electron.*, 2012, **13**, 273–282.

35 R. L. Z. Hoye, M. R. Chua, K. P. Musselman, G. Li, M. L. Lai, Z. K. Tan, N. C. Greenham, J. L. MacManus-Driscoll, R. H. Friend and D. Credgington, *Adv. Mater.*, 2015, **27**, 1414–1419.

36 J. K. Lee, W. Ma, C. J. Brabec, J. Yuen, J. Moon, J. Y. Kim, K. Lee, G. C. Bazan and A. J. Heeger, *J. Am. Chem. Soc.*, 2008, **130**, 3619–3623.

37 J. Liu, L. Chen, B. Gao, X. Cao, Y. Han, Z. Xie and L. Wang, *J. Mater. Chem. A*, 2013, **1**, 6216–6225.